Earth and Planetary Science Letters 561 (2021) 116820

Contents lists available at ScienceDirect

Earth and Planetary Science Letters

www.elsevier.com/locate/epsl

The grain growth kinetics of bridgmanite at the topmost lower mantle

Hongzhan Fei [a,*], Ulrich Faul [b], Tomoo Katsura [a,c]

HPSTAR 1273-2021

[a] Bayerisches Geoinstitut, University of Bayreuth, Bayreuth, D95447, Germany
[b] Earth Atmospheric and Planetary Sciences, Massachusetts Institute of Technology, Cambridge, MA, USA
[c] Center for High Pressure Science and Technology Advanced Research, Beijing, 100097, China

ARTICLE INFO

Article history:
Received 19 November 2020
Received in revised form 7 February 2021
Accepted 10 February 2021
Available online 18 February 2021
Editor: J. Badro

Keywords:
bridgmanite
grain growth
lower mantle

ABSTRACT

The grain size of minerals is an important parameter that controls mantle dynamics. We investigated the grain growth kinetics of bridgmanite that coexists with ferropericlase by multi-anvil experiments at 27 GPa, 1400-2400 K, corresponding to the topmost lower mantle conditions. The experimental results indicate that the grain size of bridgmanite systematically increases with increasing duration, with a grain size exponent of 5.2 ± 0.3. The grain growth rate increases with increasing temperature with an activation enthalpy of 260 ± 20 kJ/mol. The grain size of bridgmanite is ~30-45 μm in young subducted slabs at the topmost lower mantle conditions. The small grain size in subducted slabs may significantly reduce their creep strength in relatively to ambient mantle, and may cause the slab stagnation at the topmost lower mantle.

1. Introduction

Grain size of minerals is a fundamental parameter that affect geodynamic processes in the Earth's interior because it controls the physical and chemical properties of mineral aggregates including creep law, diffusive element transportation, seismic attenuation, and chemical mixing (e.g. Dannberg et al., 2017; Hirth and Kohlstedt, 2003; Faul and Jackson, 2007, 2015; Jackson et al., 2002; Lau and Faul, 2019; Solomatov and Reese, 2008; ten Grotenhuis et al., 2004). Knowledge about grain size in the Earth's interior is therefore vital to understand mantle dynamics (Dannberg et al., 2017).

The deformation mechanism in the lower mantle is dominated by either dislocation creep or diffusion creep. The absence of strong seismic anisotropy suggested that diffusion creep is more prevalent in the majority of lower mantle (e.g. Meade et al., 1995). While dislocation creep is independent of grain size, diffusion creep is inversely proportional to d^2 (Nabarro-Herring creep) or d^3 (Coble creep), where d is the average grain size. Therefore, the viscosity in the lower mantle will have a strong grain size dependence. Grain size is thus a key parameter that required for investigation of lower mantle rheology.

Because of the lack of natural samples, it is impossible to know the grain size distribution in the lower mantle directly. Instead, it can be inferred from the history of lower-mantle rocks. There are three processes that affect grain size in the lower mantle. 1) Solidification in the terrestrial magma ocean. 2) Grain size reduction to nearly zero by phase transition across the phase boundaries, i.e., dissociation of ringwoodite to bridgmanite + ferropericlase at the 660-km seismic discontinuity driven by the downward flow. 3) Grain growth over the geological time after the solidification or phase transition. Therefore, if the whole mantle convection occurs, the grain sizes of the downward flows of in the lower mantle can be estimated by the grain growth kinetics with an initial grain size of zero due to the phase transition at 660-km depth. On the other hand, if two-layer convection dominates, the grain size will follow the growth rate with initial grain size upon the origin of the rocks, e.g. formed during the solidification from magma ocean. Investigation of grain growth kinetics is thus important for understanding the properties and dynamics of the lower mantle.

Grain growth kinetics of the major upper-mantle minerals have been extensively studied (e.g., Guignard et al., 2012, 2016; Hiraga et al., 2010; Karato, 1989; Nichols and Mackwell, 1991; Nishihara et al., 2006; Tsujino and Nishihara, 2009; Yamazaki et al., 2005). Generally, they follow a power-law relationship of,

$$d^n - d_0^n = kt \quad (1)$$

where d and d_0 are the final and initial grain sizes, respectively, n is the grain size exponent (coarsening exponent), t is duration, and k is the growth rate constant, which is pressure and temperature dependent. The n exponent determines the grain size evolution with time ($d \propto t^{1/n}$ when $d_0 \ll d$). Values of 2~5 have been often observed in single phase or polymineralic system of mantle

* Corresponding author.
E-mail address: Hongzhan.fei@uni-bayreuth.de (H. Fei).

https://doi.org/10.1016/j.epsl.2021.116820
0012-821X/

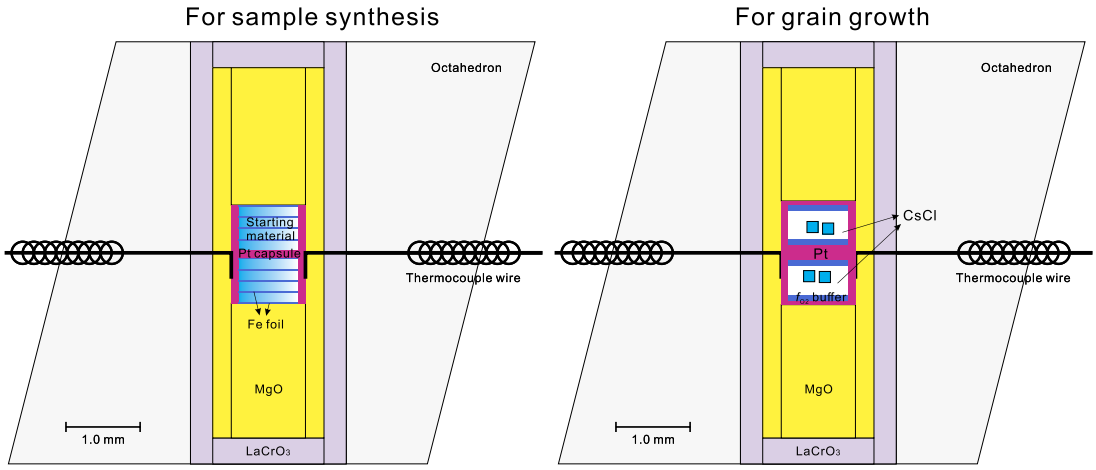

Fig. 1. Cross-sections of the cell assemblies used in this study. (a) for the sample synthesis experiment. (b) for grain growth experiments. Multiple layers of post-spinel (bridgmanite + ferropericlase) were synthesized from olivine powder using the assembly shown in (a). Each layer of the synthesized samples from (a) was cut into a number of pieces (each piece 100∼200 μm in size). The pieces were used for the grain growth experiments in (b).

minerals (e.g., Guignard et al., 2016; Hiraga et al., 2010; Nichols and Mackwell, 1991; Yamazaki et al., 2005).

In contrast to the upper mantle, the grain growth kinetics of lower mantle minerals are poorly constrained. Yamazaki et al. (1996, 2009) investigated the grain growth of bridgmanite (and periclase) at a pressure of 25 GPa and temperatures of 1570-2170 K and reported an extremely large value of n (10∼11). However, they used very fine-grained (<1 μm) Fe-free forsterite powder as a starting material, which always contains some amounts of absorbed water. Such absorbed water may enhance the grain growth of minerals significantly (e.g. Jung and Karato, 2001; Nishihara et al., 2006). Additionally, the grain growth rate of the Fe-free sample might be largely different from Fe-bearing ones (e.g. Yamazaki et al., 2005) and should be more appropriate to simulate the lower mantle. Furthermore, the non-hydrostaticity in Yamazaki et al. (1996, 2009) may affect the grain growth kinetics due to the dynamic recrystallization (Jung and Karato, 2001). Considering the nearly hydrostatic conditions in the Earth's mantle (stress at the level of 0.1∼1 MPa estimated from velocity of plate motion), experiments should be performed with minimized differential stress.

Solomatov et al. (2002) modeled the grain size evolution in the bridgmanite-ferropericlase two phase system by Monte Carlo simulation. Nevertheless, their simulations were performed based on the assumptions of $n = 4$ for a grain-boundary diffusion-controlled grain growth kinetics and $n = 3$ for a lattice diffusion-controlled process. Therefore, there is a significant gap between the experimental results and numerical simulations.

In this study, we investigated the grain growth kinetics of Fe-bearing bridgmanite that coexists with ferropericlase. The grain size of bridgmanite was measured as a function annealing duration and temperature. We also examined the effects of absorbed water and iron content. The experiments were performed at a pressure of 27 GPa with minimized stress conditions, which is smaller than 10 MPa (Rubie et al., 1993).

2. Experimental and analytical methods

2.1. Starting material

Hand-picked inclusion-free San Carlos olivine [$(Mg_{1.82}Fe_{0.18})SiO_4$] single crystals were used as a starting material in the majority of runs. The single crystals were ground to a powder with grain sizes of 1-10 μm and stored in a vacuum furnace at 400 K before use. Additionally, a piece of Fe-free forsterite single crystal [Mg_2SiO_4, impurity described in Fei et al. (2012)] was used to examine the iron effect.

2.2. Sample syntheses of high-pressure phase assemblages

Bridgmanite samples coexisting with ferropericlase were synthesized from the San Carlos olivine powder using a multi-anvil press. Multiple layers of olivine powder separated by Fe foils were loaded into a Pt capsule with outer and inner diameters of 1.0 and 0.8 mm, respectively. The thickness of each layer was about 150 μm (Fig. 1a). Tiny amounts of Fe-FeO (IW buffer) was loaded next to the Fe foils to fix the oxygen fugacity (f_{O2}). The capsule was loaded into a 7/3 standard multi-anvil cell assembly at the Bayerisches Geoinstitut with a $LaCrO_3$ furnace, a Cr_2O_3-doped MgO octahedron with 7-mm edge length, and a D-type W/Re thermocouple (Fig. 1).

The completed whole assembly was dried in a vacuum furnace at 400 K for over 24 hours. Afterwards, it was compressed to 27 GPa at room temperature by 8 pieces of tungsten carbide cubes with 26-mm edge lengths and 3-mm truncation edge lengths using a 15-MN multi-anvil press with the Osugi-type guide block at the Bayerisches Geoinstitut (Ishii et al., 2019). After reaching the desired pressure, the assembly was heated to 1700 K with a ramping rate of ∼50 K/min. After keeping the temperature at 1700 K for 5 min, the assembly was quenched to room temperature by switching off the heating power and decompressed slowly to ambient pressure over more than 15 hours.

Finally, well-sintered and homogeneously distributed aggregates of bridgmanite-ferropericlase mixtures (hereafter post-spinel) with grain sizes less than 0.1 μm were obtained (Fig. 2). Each layer was mechanically broken into small pieces with 100-200 μm in size using a razor under an optical microscope. The small pieces were used as samples in the following grain growth experiments.

2.3. Grain-growth experiments

In each grain growth run, pieces of the synthesized post-spinel aggregates were embedded in a pre-dried CsCl powder within Pt capsule, which provided quasi-hydrostatic conditions (e.g., Fei et al., 2017). A Fe-FeO powder (IW buffer) was loaded at the two ends of Pt capsule to buffer the f_{O2}. The capsule was loaded into the standard 7/3 multi-anvil assembly again (Fig. 1b), and dried in a desiccator before compression. The grain growth runs were performed at a pressure of 27 GPa and temperatures of 1400 to 2400 K following the same compression and heating procedure as

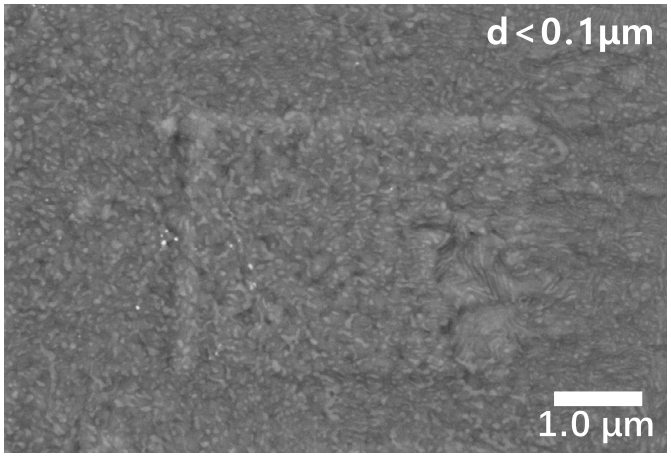

Fig. 2. Synthesized post-spinel for grain growth runs. Because of bridgmanite amorphousization, it is unable to take high magnification images for statistic analysis of grain size, but it is clearly less than 0.1 μm, which is much smaller than those after grain growth runs as listed in Table 1.

Table 1
A list of run conditions, results of bridgmanite grain sizes in the run products, and the growth rate. All experiments were performed at a pressure condition of 27 GPa. d: grain size. k: grain growth rate constant. IW: Fe-FeO buffer. The post-spinel is pre-synthesized from San Carlos olivine.

Run No.	T (K)	Duration (min)	f_{O2} buffer	Sample	Analyzed BSE images	Analyzed grains (N)	Log d (μm)	$\bar{d}$ (μm)	k ($\mu m^n/s$)
I930-Ol-R	2200	1000	IW	Post-spinel	5	756	0.23 (15)	1.72	2.77×10^{-4}
I951-Ol-R	2200	10	IW	Post-spinel	3	843	−0.14 (15)	0.72	3.02×10^{-4}
I928-Ol-R	2200	1.5	IW	Post-spinel	3	883	−0.38 (14)	0.42	1.22×10^{-4}
I959-Ol-R	2200	100	IW	Post-spinel	3	474	−0.03 (11)	0.94	1.18×10^{-4}
I957-Ol-R	1800	1000	IW	Post-spinel	3	365	−0.06 (13)	0.87	7.98×10^{-6}
I958-Ol-R	2000	1000	IW	Post-spinel	3	369	0.07 (13)	1.17	3.85×10^{-5}
I956-Ol-R	2000	10	IW	Post-spinel	4	916	−0.23 (15)	0.59	1.11×10^{-4}
I997-Ol-R	2400	60	IW	Post-spinel	3	434	0.09 (14)	1.24	8.52×10^{-4}
I937-Ol-R	1400	1000	IW	Post-spinel	3	304	−0.49 (12)	0.33	4.94×10^{-8}
I1023-Ol	2200	100	IW	Post-spinel	3	447	0.03 (17)	1.08	2.44×10^{-4}
I1105[*a]	2200	5	No	Olivine powder	5	340	−0.10 (13)	0.79	–[*b]
				Post-spinel	4	397	−0.24 (15)	0.57	1.79×10^{-4}
				Olivine single crystal	4	320	−0.24 (13)	0.58	1.91×10^{-4}
				Forsterite single crystal	4	537	−0.33 (12)	0.47	5.30×10^{-5}
I1143[*a]	2200	300	No	Olivine powder	4	327	0.09 (12)	1.24	–[*b]
				Post-spinel	3	456	0.08 (8)	1.21	1.49×10^{-4}
				Forsterite single crystal	3	349	−0.02 (12)	0.95	4.29×10^{-5}
I1147[*a]	2200	2	No	Olivine powder	4	364	−0.13 (15)	0.75	–[*b]
				Post-spinel	3	318	−0.33 (12)	0.47	1.60×10^{-4}
				Forsterite single crystal	3	591	−0.43 (12)	0.38	3.83×10^{-5}

[*a] Two capsules (in total four samples) were loaded in these runs. The first capsule is filled with olivine powder without CsCl. The second capsule contains multiple samples, i.e., post-spinel, olivine single crystal, and Fe-free forsterite single crystal embedded in CsCl. Only the post-spinel sample in the second capsule was pre-synthesized.
[*b] Because the grain size exponent of the olivine powder samples is supposed to be affected by absorbed water, the k is not calculated here.

that for sample synthesis experiment. The annealing durations of the grain growth runs were from 1.5 to 1000 min as listed in Table 1.

To examine possible effects of Fe content and absorbed water in Yamazaki et al. (1996)'s experiments, three additional runs (I1105, I1143, I1147 in Table 1) were performed at a pressure of 27 GPa and a temperature of 2200 K for 2-300 min of annealing duration. In these runs, two capsules were loaded in the same assembly. The first capsule was filled with San Carlos olivine powder, which is expected to contain absorbed water. The second capsule contained multiple pieces of samples embedded in CsCl, i.e., pre-synthesized post-spinel aggregates, San Carlos olivine single crystal, and Fe-free forsterite single crystal.

2.4. Grain-size measurements

The recovered samples were carefully taken out from CsCl by dissolving it in water, mounted and polished by emery papers and 0.25 μm diamond pastes, and imaged using a scanning electron microscope (SEM) with acceleration voltages of 5 to 20 kV. The grains were hand-traced in the BSE images and the area of each bridgmanite grain was obtained by image processing software ImageJ (https://imagej.nih.gov/ij/). The diameter of each grain was calculated from the area by approximating the grain shape by a circle. More than three BSE images from different regions of each sample were analyzed, for a total of more than 300 bridgmanite grains. The grain size of ferropericlase was not investigated in this study.

3. Experimental results

3.1. Grain size distribution

Bridgmanite and ferropericlase phases are clearly distinguished by brightness contrast in back-scattered electron (BSE) images. Bridgmanite grains have sharp grain boundaries and 120°-angle

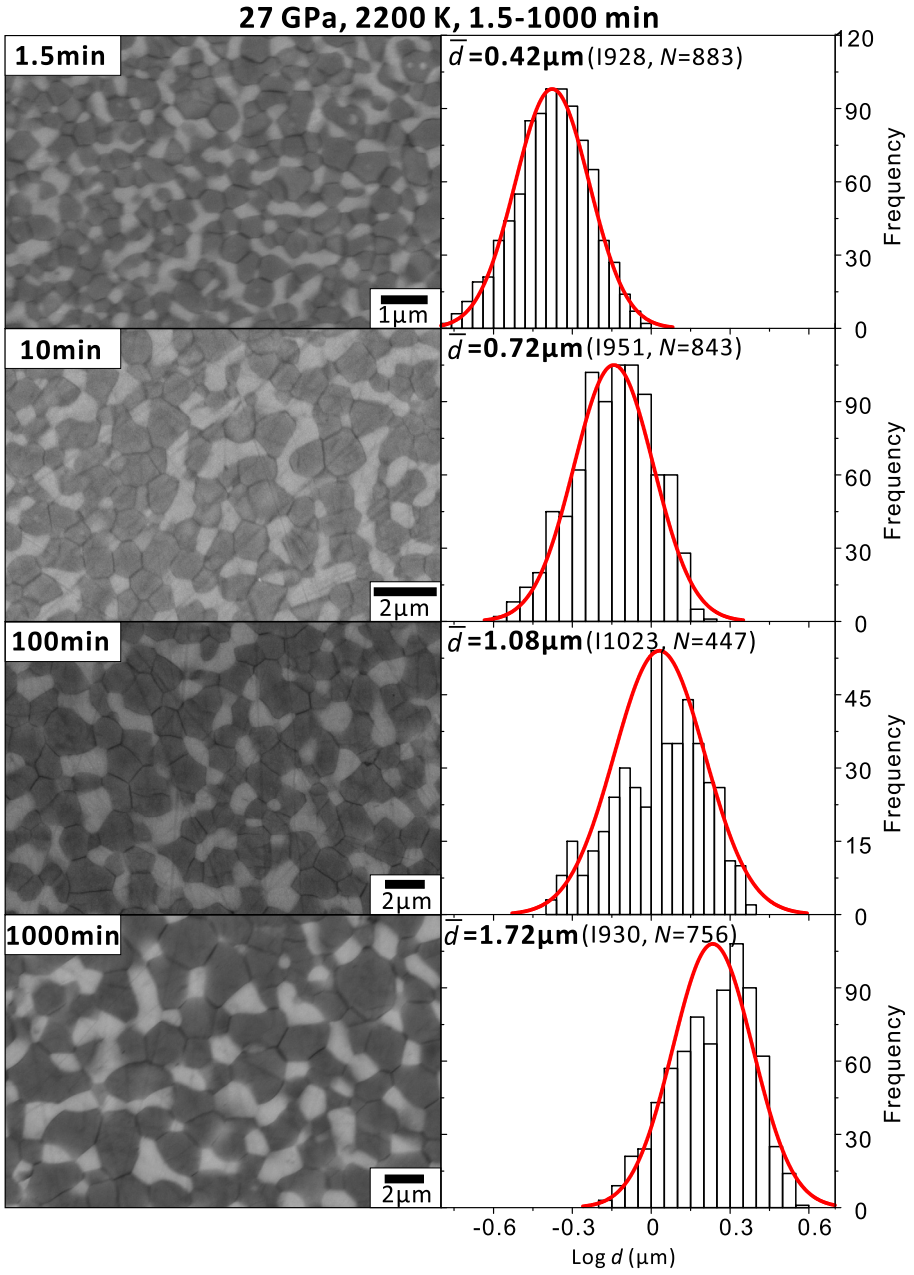

Fig. 3. BSE images (left) and grain size distributions (right) of the samples annealed at the same pressure and temperature conditions (27 GPa, 2200 K), but different run durations (1.5 to 1000 min). The grain size of bridgmanite (dark grains) show relatively narrow and symmetric Gaussian distributions. The average grain size ($\bar{d}$) increases systematically with increasing annealing duration. High resolution BSE images are given in the online Supplementary Material.

triple junctions (e.g. Fig. 3). No clearly heterogeneous grain size distribution was found. With a sufficiently large number (>300) of analyzed grains for each sample, the grain sizes in log unit ($\log d$) show a relatively narrow and symmetric Gaussian distributions (Fig. 3). The mean values and standard deviations of $\log d$ were thus obtained from the Gaussian distributions and listed in Table 1.

3.2. Grain size exponent

Examples of BSE images obtained from samples annealed at the same pressure (27 GPa) and temperature (2200 K) conditions but with different durations are shown in Fig. 3. The grain size of bridgmanite systematically increases from 0.42 μm to 0.72, 1.08, and 1.69 μm with increasing duration from 1.5 min to 10, 100, and 1000 min, respectively. The $\log d$ of bridgmanite was plotted against $\log t$ in Fig. 4. Overall, $\log d$ is found to be linearly correlated with $\log t$. Because d_0 (<0.1 μm) is negligible in comparison with d, the data points are fit to equation (1) in the form of,

$$\left(\frac{\partial(\log d)}{\partial(\log t)}\right)_T = \frac{1}{n} \tag{2}$$

and a grain size exponent of $n = 5.2 \pm 0.3$ is obtained by the least square fitting.

3.3. Grain growth rate constant

For experiments performed with the same duration (1000 min), at a range of temperature conditions, the grain size of bridgmanite increases from 0.33 to 1.72 μm with increasing temperature from 1400 to 2200 K (Fig. 5). Grain growth rate constants (k) were

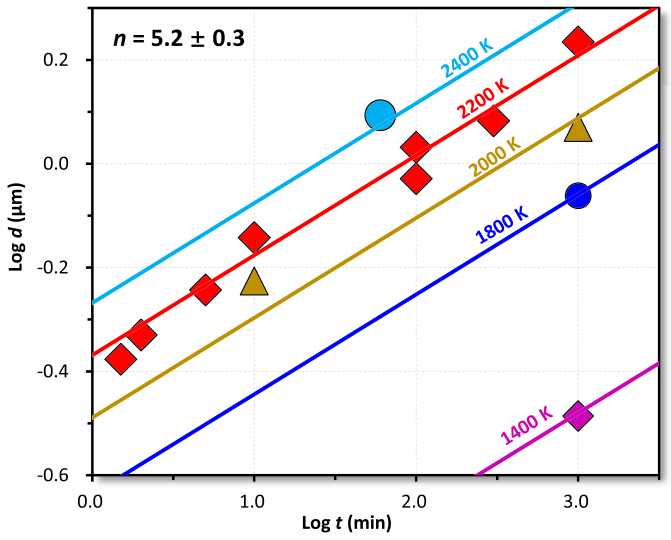

Fig. 4. Bridgmanite grain size evolution with time at 1400-2400 K. The slope of the fitting lines represents $1/n$ in Eq. (2).

calculated from Eq. (1) with the above determined grain size exponent of 5.2 and the results are listed in Table 1. The values of k are plotted as a function of temperature in Fig. 6. Since grain growth is a kinetic process, k should follow the Arrhenius relation,

$$k = k_0 \exp\left(-\frac{\Delta H}{RT}\right) \quad (3)$$

where k is in $\mu m^n/s$, k_0 is the pre-exponential factor, ΔH is the activation enthalpy, R is the ideal gas constant, and T is absolute temperature. Least squares fitting to Eq. (2) yields $\log k_0$ ($\mu m^n/s$) $= 2.6 \pm 0.4$ and $\Delta H = 260 \pm 20$ kJ/mol.

4. Discussion

4.1. Comparison with previous studies

The grain size exponent determined in this study is 5.2 ± 0.3. It is much smaller than that determined by Yamazaki et al. (1996), which was 10.6 ± 1.1 (Fig. 4). Namely, the grain size of bridgmanite has much stronger time-dependence than previously thought. This difference should not be caused by experimental uncertainty, because the scatters of $\log d$ are within 0.1 log unit in both this study and in Yamazaki et al. (1996), whereas the difference between this study and Yamazaki et al. (1996) is larger than 0.3 log unit in short-duration experiments (Fig. 4).

As explained in the introduction section, the extremely large n obtained by Yamazaki et al. (1996) could be caused by the effects of absorbed water and/or iron because they used fine-grained Fe-free forsterite powder samples. To examine our hypotheses, the I1105, I1143, and I1147 were performed with multiple samples in each run (Table 1). Because the multiple samples should experience exactly the same P-T condition and the same duration in each run, they can be directly compared with minimized experimental uncertainties. As shown in Fig. 7 and Fig. 8, the samples initially from the olivine single crystal and from the pre-synthesized post-spinel have exactly the same grain sizes. This is reasonable because both of them are dry and have the same composition. When the annealing duration is short (2 and 5 mins in I1147 and I1105, respectively), the samples from the olivine powder have larger grain sizes than those from pre-synthesized post-spinel. In contrast, when the heating duration is long (300 min in I1143), the difference diminished. Fe-free forsterite single crystal sample has smaller grain size than iron-bearing system, indicating that presence of Fe enhances the grain growth of bridgmanite.

The $\log d$ vs. $\log t$ from forsterite single crystals indicates $n = 5.5 \pm 0.4$, which is identical to the Fe-bearing system, but smaller than the value of 10.6 ± 1.1 determined by Yamazaki et al. (1996) with forsterite powder as the starting material (Fig. 8). Our olivine powder samples show $n = 9.7 \pm 0.6$ (dot line in Fig. 8), which is much larger than the pre-synthesized post-spinel samples and comparable with Yamazaki et al. (1996). Therefore, we interpret that, when powder samples were used, the grain growth was significantly enhanced by absorbed water in short duration experiments, but such an effect diminished in long duration experiments due to sample dehydration. As a result, the grain size exponent was apparently enlarged. Because the Pt capsules were not welded, water should have escaped from the capsules continuously, therefore, the $\log d$ vs. $\log t$ relation should be curved (dashed line in Fig. 8). Since the powder used in Yamazaki et al. (1996) had less than 1- μm particle size, and our olivine powder is 1-10 μm, the absorbed water will be different by a factor of ~10 by assuming the one order of magnitude difference in particle size. Using the water exponent of 1.7 of a wet system (Nishihara et al., 2006), the grain size could be raised by ~0.33 log units, which explains the discrepancy of $\log d$ between this study and Yamazaki et al. (1996). Of course the above scenario is our interpretation based on Fig. 8 and the exact reason for the discrepancy is unknown. It nevertheless well explains the discrepancy of both n and $\log d$ and therefore we believe it is the most convincing reason.

4.2. Grain growth mechanisms

Theoretically, the grain growth of polycrystalline aggregates occurs by the migration of grain boundaries. It should be controlled by the atomic diffusion of the slowest elements. In two-phase systems, the grain size exponents are generally $n = 3$ when grain growth is controlled by lattice diffusion, $n = 4$ when controlled by grain-boundary diffusion, and $n \geq 5$ when controlled by diffusion along dislocations (pipe diffusion) (Atkinson, 1988; Ardell, 1972; Brook, 1976). Additionally, the elastic stress in high-pressure experiments may also affect the value of grain size exponent (Solomatov et al., 2002).

Because the samples were surrounded by CsCl in this study, the non-hydrostatic stress should be minimal, i.e., resulting in anni-

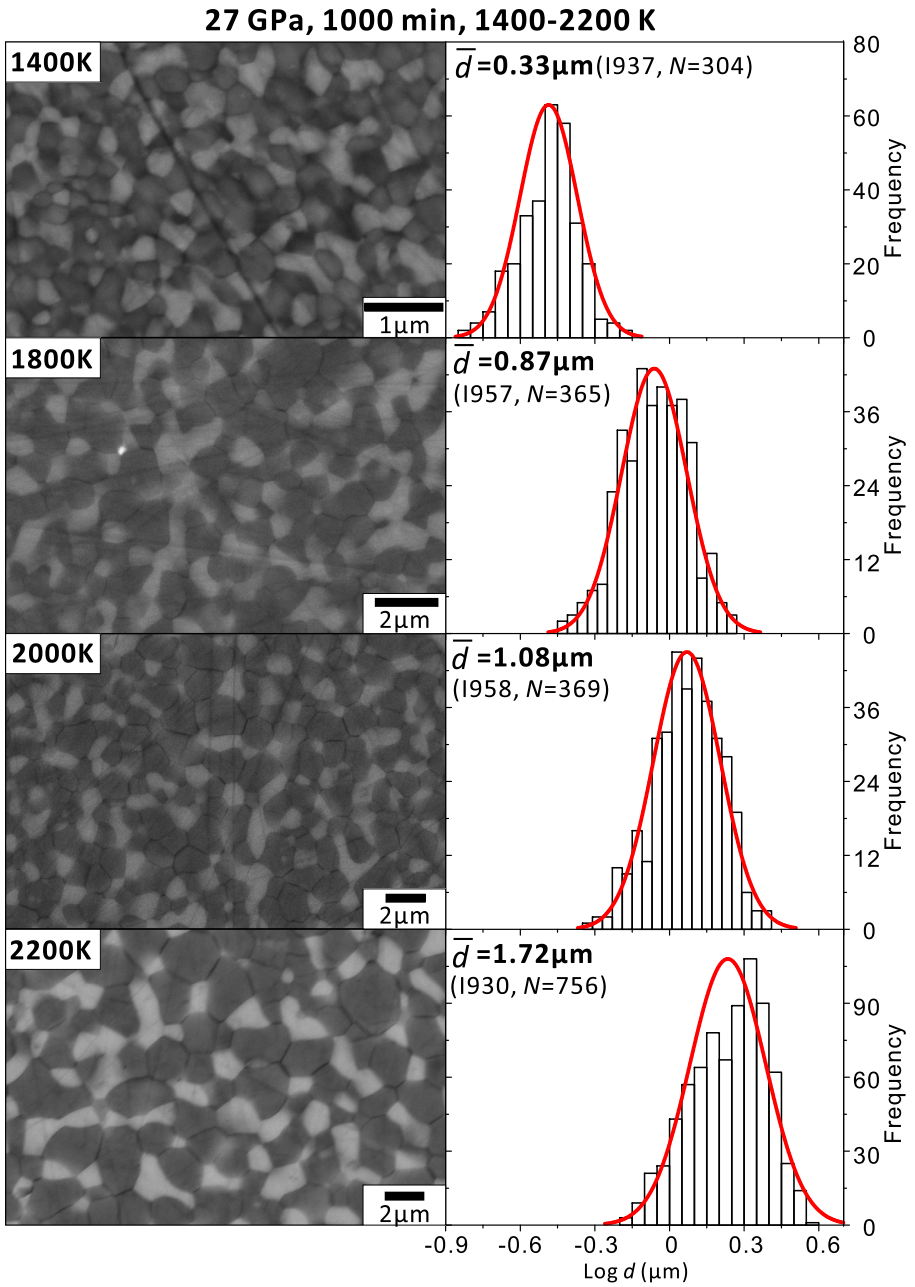

Fig. 5. BSE images (left) and grain size distributions (right) of the samples annealed at 27 GPa with the same run duration (1000 min), but different temperatures (1400-2200 K). The average grain size ($\bar{d}$) increases systematically with increasing temperature. High resolution BSE images are given in the online Supplementary Material.

hilation of dislocations. Therefore, the dislocation density should be extremely low (Fei et al., 2017). Thus, the grain growth mechanism in this study with $n = 5.2 \pm 0.3$ should not be influenced by stress or dislocation-controlled diffusion. Hiraga et al. (2010) reported a value of $n \approx 5$ in the forsterite-enstatite system, which is comparable as the n determined in this study for the bridgmanite-ferropericlase system. They found that the experimentally measured grain growth rates in the forsterite-enstatite system are comparable with those simulated from Si grain-boundary diffusion coefficients. Therefore, they concluded that grain-boundary diffusion controlled grain growth even though the grain size exponent is n ≈ 5. Considering the grain size exponent of $n = 5.2 \pm 0.3$ determined in this study and that it is unlikely that stress or dislocation-controlled diffusion influenced the growth rates as explained above, we conclude that the grain growth process of bridgmanite in this study is controlled by the grain boundary diffusion as well. Therefore, k should be proportional to D^{gb}, where D^{gb} is the grain boundary diffusion coefficient of the slowest species.

The Mg grain boundary diffusion coefficient in bridgmanite is unknown, but it is expected to be similar to Si, because they have nearly identical lattice diffusion coefficients (Dobson et al., 2008; Holzapfel et al., 2005; Xu et al., 2011; Yamazaki et al., 2000). On the other hand, the oxygen grain-boundary diffusion is 3-4 orders of magnitude faster than Si (Dobson et al., 2008; Yamazaki et al., 2000). Thus, Si and Mg should be the rate-limiting species for grain growth of bridgmanite. This is also suggested by the comparable activation enthalpy for Si grain boundary diffusion (310±50 kJ/mol determined in Yamazaki et al., 2000), for grain-boundary controlled anelastic process (286 kJ/mol, Lau and Faul, 2019), and for grain growth process (260 ± 20 kJ/mol determined in this study).

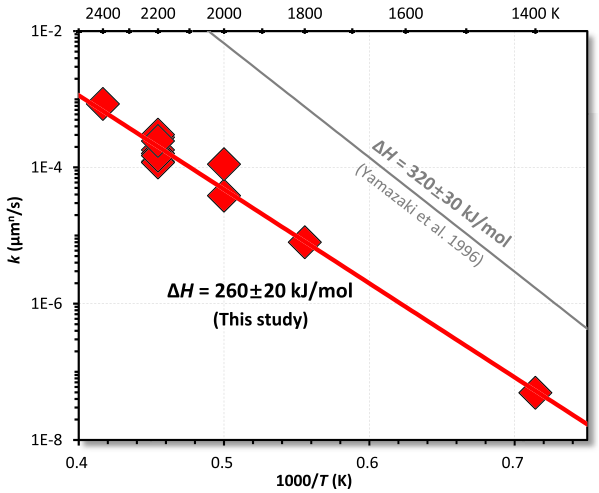

Fig. 6. The grain growth rate of bridgmanite phase in post-spinel as a function of temperature at 27 GPa. The fit to the experimental results given by Yamazaki et al. (1996) is also shown for comparison.

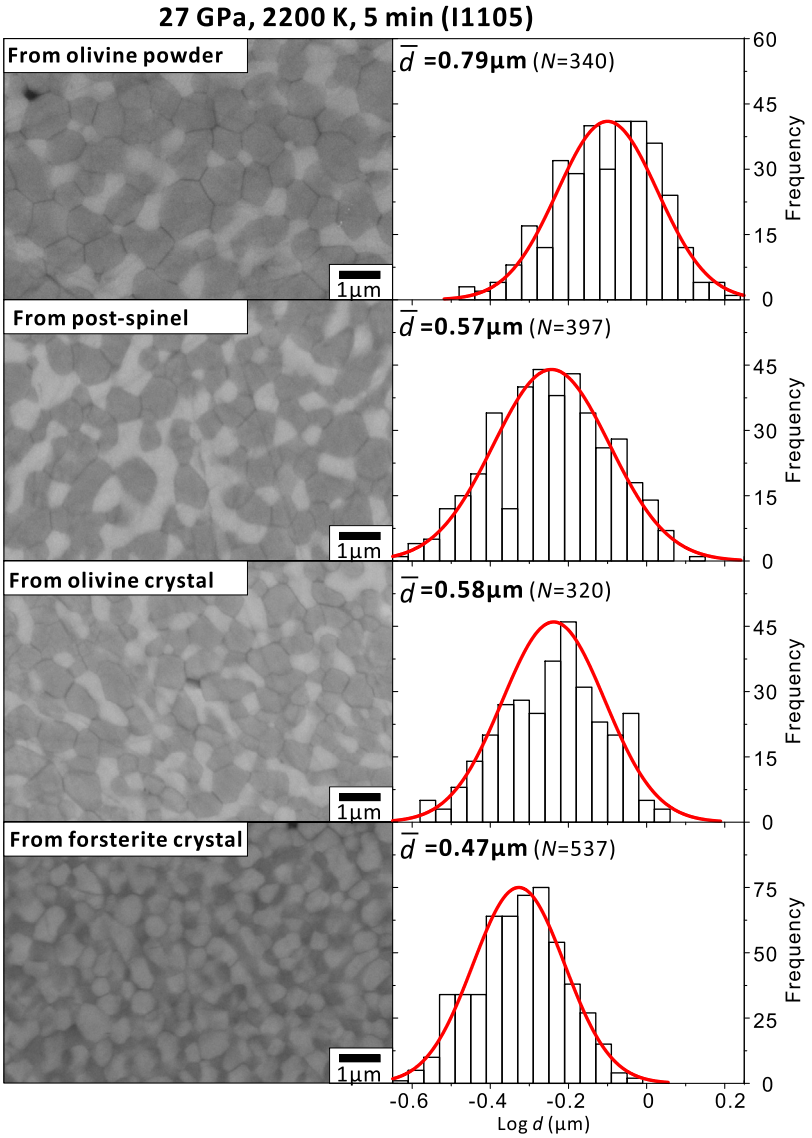

Fig. 7. BSE images (left) and grain size distributions (right) of the samples recovered from run I1105 (2200 K, 5 min) with different starting materials (olivine powder, pre-sintered post-spinel, olivine single crystal, and Fe-free forsterite single crystal). Because the four samples experience exactly the same pressure, temperature, and duration conditions, they can be compared directly with minimized uncertainty even though the differences of log$d$ among them are not large. High resolution BSE images are given in the online Supplementary Material.

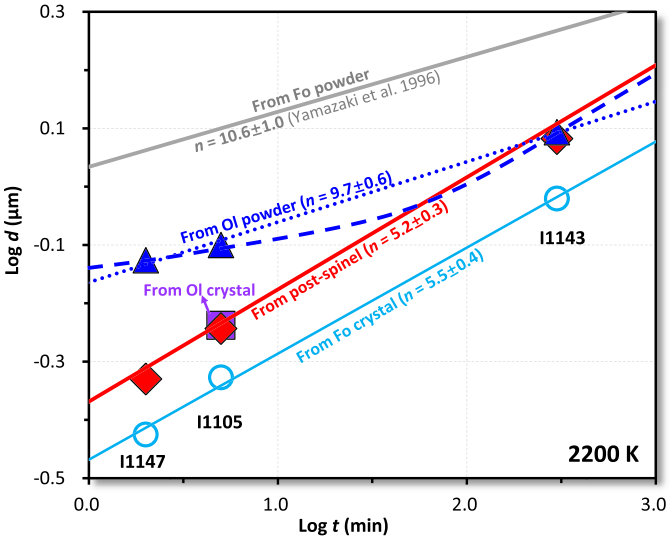

Fig. 8. A comparison of grain sizes with different types of starting materials (olivine powder, olivine single crystal, pre-synthesized post-spinel, and Fe-free forsterite single crystal) in run I1147 (2 min), I1105 (5 min) and I1143 (300 min) and with forsterite powder from Yamazaki et al. (1996). Ol: San Carlos olivine. Fo: Fe-free forsterite.

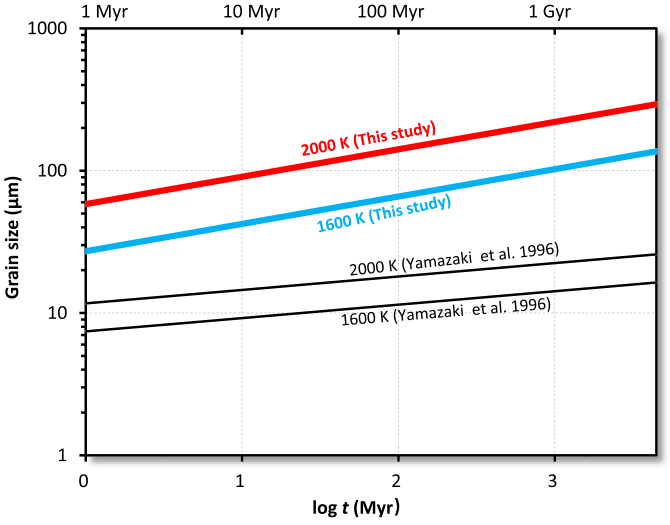

Fig. 9. Grain sizes of bridgmanite at the topmost of the lower mantle for different temperatures as a function of geological time. The grain sizes based on Yamazaki et al. (1996) are also shown for comparison.

4.3. Grain size at the topmost lower mantle

Although the grain size of bridgmanite in Yamazaki et al. (1996) is larger than that of the present study in the investigated annealing durations (Fig. 4), the relations will be reversed with longer duration due to their large grain growth exponent. The crossover will occur at an annealing time of $\sim 10^4$-10^5 min (10^1-10^2 days). The grain size of bridgmanite at geological time scales should therefore be much larger than previously considered.

Because of the phase transformation across the 660-km discontinuity in subducted slabs, the grain size of bridgmanite in the topmost lower mantle can be estimated based on the grain growth rate determined in this study and initial grain size of zero due to the phase transformation. By assuming a slab geotherm of 1600 K at 700 km depth [400 K lower than the mantle geotherm (e.g. Fukao et al., 2009; Schmid et al., 2006)], over a geological time of 1-10 Myr (corresponding to tens to hundreds kilometer subduction depth), the grain size of bridgmanite will be 30∼45 μm (Fig. 8). It is about 0.5 order of magnitude larger than that calculated from Yamazaki et al. (1996) (∼10 μm for 1-10 Myr age at 1600 K) (Fig. 8). Consequently, since diffusion creep is inversely proportional to d^2∼d^3, the diffusion creep rate in the slabs mantle should be 1∼1.5 orders of magnitude lower than that estimated using Yamazaki et al. (1996)'s results.

The grain size in the ambient mantle will follow the growth rate with an initial grain size determined by the origin and history of the rocks. If we assume the minimum case, i.e., initial grain size of zero, over a geological time of 100 Myr – 1 Gyr at the topmost lower mantle temperature [2000 K, Katsura et al., 2010)], the grain size will be 150-230 μm (Fig. 9). It is larger than the subducted slabs by a factor of 3∼10. The grain size effect will therefore increase the diffusion creep rate of slabs at least by one order of magnitude in comparison with the ambient mantle. On the other hand, the observations of seismic anisotropies around slabs imply the contribution of dislocation creep in these regions (e.g. Foley and Long, 2011; Lynner and Long, 2014; Meade et al., 1995). Namely, the contribution of dislocation creep will further lower the slab strength. Therefore, the subducted slabs are expected to be softer than ambient mantle. This could be one reason that some subducted slabs stagnate below the 660-km discontinuity (e.g. Fukao and Obayashi, 2013).

CRediT authorship contribution statement

Hongzhan Fei: Conceptualization, Formal analysis, Investigation, Methodology, Validation, Visualization, Writing – original draft, Writing – review & editing. **Ulrich Faul:** Conceptualization, Methodology, Writing – review & editing. **Tomoo Katsura:** Conceptualization, Funding acquisition, Project administration, Writing – review & editing.

Declaration of competing interest

The authors declare that they have no known competing financial interests or personal relationships that could have appeared to influence the work reported in this paper.

Acknowledgements

This work is supported by the Advanced Grant of the European Research Council (ERC) under the European Union's Horizon 2020 research and innovation program (No. 787527), the research grant of Deutsche Forschungsgemeinschaft (DFG) (KA3434/9-1, KA3434/11-1, and KA3434/12-1), and the annual budget of Bayerisches Geoinstitut.

Appendix A. Supplementary material

Supplementary material related to this article can be found online at https://doi.org/10.1016/j.epsl.2021.116820.

References

Atkinson, H.V., 1988. Theories of normal grain growth in pure single phase systems. Acta Metall. 36, 469–491.
Ardell, A., 1972. On the coarsening of grain boundary precipitates. Acta Metall. 20, 601–609.
Brook, R.J., 1976. Controlled grain growth. Treatise Mater. Sci. Technol. 9, 331–364.
Dannberg, J., Eilon, Z., Faul, U., Gassmoller, R., Moulik, P., Myhill, R., 2017. The importance of grain size to mantle dynamics and seismological observations. Geochem. Geophys. Geosyst. 18, 3034–3061.
Dobson, D.P., Dohmen, R., Wiedenbeck, M., 2008. Self-diffusion of oxygen and silicon in $MgSiO_3$ perovskite. Earth Planet. Sci. Lett. 270, 125–129.
Faul, U., Jackson, I., 2015. Transient creep and strain energy dissipation: an experimental perspective. Annu. Rev. Earth Planet. Sci. 43, 541–569.
Faul, U., Jackson, I., 2007. Diffusion creep of dry, melt-free olivine. J. Geophys. Res. 112, B04204.

Fei, H., Hegoda, C., Yamazaki, D., Wiedenbeck, M., Yurimoto, H., Shcheka, S., Katsura, T., 2012. High silicon self-diffusion coefficient in dry forsterite. Earth Planet. Sci. Lett. 345, 95–103.

Fei, H., Yamazaki, D., Sakurai, M., Miyajima, N., Ohfuji, H., Katsura, T., Yamamoto, T., 2017. A nearly water-saturated mantle transition zone inferred from mineral viscosity. Sci. Adv. 3, e1603024.

Foley, B.J., Long, M.D., 2011. Upper and mid-mantle anisotropy beneath the Tonga slab. Geophys. Res. Lett. 38, L02303.

Fukao, Y., Obayashi, M., Nakakuki, T., Deep Slab Project Group, 2009. Stagnant slab: a review. Annu. Rev. Earth Planet. Sci. 37, 19–46.

Fukao, Y., Obayashi, M., 2013. Subducted slabs stagnant above, penetrating through, and trapped below the 660 km discontinuity. J. Geophys. Res. 118, 5920–5938.

Guignard, J., Bystricky, M., Toplis, M.J., 2012. Grain growth in forsterite-nickel mixtures: analogues of small parent bodies during early accretion. Phys. Earth Planet. Inter. 204, 37–51.

Guignard, J., Toplis, M.J., Bystricky, M., Monnereau, M., 2016. Temperature dependent grain growth of forsterite-nickel mixtures: implications for grain growth in two-phase systems and applications to the H-chondrite parent body. Earth Planet. Sci. Lett. 443, 20–31.

Hirth, G., Kohlstedt, D., 2003. Rheology of the upper mantle and mantle wedge: a view from the experimentalists. Geophys. Monogr. 138, 83–105.

Hiraga, T., Tachibana, C., Ohashi, N., Sano, S., 2010. Grain growth systematics for forsterite ± enstatite aggregates: effect of lithology on grain size in the upper mantle. Earth Planet. Sci. Lett. 29, 10–20.

Holzapfel, C., Rubie, D.C., Frost, D.J., Langenhorst, F., 2005. Fe-Mg interdiffusion in (Mg, Fe)SiO_3 perovskite and lower mantle reequilibration. Science 309, 1707–1710.

Ishii, T., Liu, Z., Katsura, T., 2019. A breakthrough in pressure generation by a Kawai-type multi-anvil apparatus with tungsten carbide anvils. Engineering 5, 434–440.

Jackson, I., Gerald, J.D.F., Faul, U.H., Tan, B.H., 2002. Grain-size-sensitive seismic wave attenuation in polycrystalline olivine. J. Geophys. Res. 107, 2360. https://doi.org/10.1029/2001JB001225.

Jung, H., Karato, S.I., 2001. Effects of water on dynamically recrystallized grain-size of olivine. J. Struct. Geol. 23, 1337–1344.

Karato, S., 1989. Grain growth kinetics in olivine aggregates. Tectonophysics 168, 255–273.

Katsura, T., Yoneda, A., Yamazaki, D., Yoshino, T., Ito, E., 2010. Adiabatic temperature profile in the mantle. Phys. Earth Planet. Inter. 183, 212–218.

Lau, H.C.P., Faul, U.H., 2019. Anelasticity from seismic to tidal timescales: theory and observations. Earth Planet. Sci. Lett. 508, 18–29.

Lynner, C., Long, M.D., 2014. Sub-slab anisotropy beneath the Sumatra and circum-Pacific subduction zones from source-side shear wave splitting observations. Geochem. Geophys. Geosyst. 15, 2262–2281.

Meade, C., Silver, P.G., Kaneshima, S., 1995. Laboratory and seismological observations of lower mantle isotropy. Geophys. Res. Lett. 22, 1293–1296.

Nichols, S.J., Mackwell, S.J., 1991. Grain growth in porous olivine aggregates. Phys. Chem. Miner. 18, 269–278.

Nishihara, Y., Shinmei, T., 2006, Karato Grain-growth kinetics in wadsleyite: effect of chemical environment. Phys. Earth Planet. Inter. 154, 30–43.

Rubie, D.C., Karato, S., Yan, H., O'Neill, H.S.C., 1993. Low differential stress and controlled chemical environment in Multianvil high-pressure experiments. Phys. Chem. Miner. 20, 315–322.

Schmid, C., van der Lee, S., Giardini, D., 2006. Correlated shear and bulk moduli to 1400 km beneath the Mediterranean region. Phys. Earth Planet. Inter. 159, 213–224.

Solomatov, V.S., El-Khozondar, R., Tikare, V., 2002. Grain size in the lower mantle: constraints from numerical modeling of grain growth in two-phase systems. Phys. Earth Planet. Inter. 129, 265–282.

Solomatov, V.S., Reese, C.C., 2008. Grain size variations in the Earth's mantle and the evolution of primordial chemical heterogeneities. J. Geophys. Res. 113, B07408.

ten Grotenhuis, S.M., Drury, M.R., Peach, C.J., Spiers, C.J., 2004. Electrical properties of fine-grained olivine: evidence for grain boundary transport. J. Geophys. Res. 109, B06203.

Tsujino, N., Nishihara, Y., 2009. Grain-growth kinetics of ferropericlase at high-pressure. Phys. Earth Planet. Inter. 174, 145–152.

Xu, J., Yamazaki, D., Katsura, T., Wu, X., Remmert, P., Yurimoto, H., Chakraborty, S., 2011. Silicon and magnesium diffusion in a single crystal of $MgSiO_3$ perovskite. J. Geophys. Res. 116, B12205.

Yamazaki, D., Kato, T., Ohtani, E., Toriumi, M., 1996. Grain growth rates of $MgSiO_3$ perovskite and periclase under lower mantle conditions. Science 274, 2052–2054.

Yamazaki, D., Kato, T., Yurimoto, H., Ohtani, E., Toriumi, M., 2000. Silicon self-diffusion in $MgSiO_3$ perovskite at 25 GPa. Phys. Earth Planet. Inter. 119, 299–309.

Yamazaki, D., Inoue, T., Okamoto, M., Irifune, T., 2005. Grain growth kinetics of ringwoodite and its implication for rheology of the subducting slabs. Earth Planet. Sci. Lett. 236, 871–881.

Yamazaki, D., Yoshino, T., Matsuzaki, T., Katsura, T., Yoneda, A., 2009. Texture of (Mg, Fe)SiO_3 perovskite and ferro-periclase aggregate: implications for rheology of the lower mantle. Phys. Earth Planet. Inter. 174, 138–144.